

# Mechanistic insights and selected synthetic routes of atomically precise metal nanoclusters

Mustafa Gharib<sup>1,2</sup> | Michael Galchenko<sup>3</sup> | Christian Klinke<sup>4,5</sup> |  
Wolfgang J. Parak<sup>1,6</sup>  | Indranath Chakraborty<sup>1</sup> 

<sup>1</sup> Fachbereich Physik, Center for Hybrid Nanostructures (CHyN), Universität Hamburg, Hamburg, Germany

<sup>2</sup> Radiation Biology Department, Egyptian Atomic Energy Authority (EAEA), Cairo, Egypt

<sup>3</sup> Fachbereich Chemie, Universität Hamburg, Hamburg, Germany

<sup>4</sup> Institute of Physics, University of Rostock, Albert-Einstein-Strasse 23, Rostock, Germany

<sup>5</sup> Department of Chemistry, Swansea University – Singleton Park, Swansea, UK

<sup>6</sup> CIC Biomagune, San Sebastian, Spain

## Correspondence

Indranath Chakraborty, Fachbereich Physik, Center for Hybrid Nanostructures (CHyN), Universität Hamburg, 22761 Hamburg, Germany.  
Email: [indranath.chakraborty@physik.uni-hamburg.de](mailto:indranath.chakraborty@physik.uni-hamburg.de)

## Abstract

During the last few decades, noble metal nanoclusters (NCs) have become an exciting building block in the field of nanoscience. With their ultrasmall size that ranges between 1 and 2 nm, NCs fill the gap between atoms and nanoparticles (NPs), and they show significantly different physicochemical properties compared to their bulk counterparts, such as molecule-like HOMO-LUMO discrete electronic transitions, photoluminescence, etc. These properties made NCs potential candidates in various applications, including catalysis, chemical/bioimaging, biomedicine, sensing, and energy conversion. Controlling the size of NPs, which usually exhibit a degree of polydispersity, has been a significant challenge for nano-scientists. However, metal NCs with atomic precision pave the way to accurately fabricate NPs based on an atom-by-atom assembly. This Perspective is directed to the community of nano-scientists interested in the field of NCs and summarizes the most commonly used synthetic routes of atomically precise metal NCs. Moreover, this Perspective provides an understanding of the different techniques used to control the size of metal NCs with insights on switching the surface ligands from phosphine to thiol. This Perspective also explains the role of physicochemical parameters in different synthetic routes such as high-temperature route, CO-directed route, solid-state route, ligand-exchange-induced size/structure transformation (LEIST), etc. We finally give a brief outlook on future challenges of currently used synthetic routes with some suggestions to improve them.

## KEYWORDS

atomically precise materials, formation mechanism, metal nanoclusters, synthesis methods, thiolated nanoclusters

This is an open access article under the terms of the [Creative Commons Attribution](https://creativecommons.org/licenses/by/4.0/) License, which permits use, distribution and reproduction in any medium, provided the original work is properly cited.

© 2021 The Authors. *Nano Select* published by Wiley-VCH GmbH

## 1 | INTRODUCTION

Nanomaterials are exciting building blocks of modern science and technology owing to their particular size-dependent properties.<sup>[1]</sup> Noble metal nanoparticles (NPs) have evolved significantly (particularly in terms of surface modifications<sup>[2]</sup>) after the pioneer studies of Faraday's "colloidal gold."<sup>[3]</sup> Controlling the size of NPs is very important to understand the mechanistic details of their interesting properties. Diverse methodologies have been developed to synthesize NPs of controlled sizes.<sup>[4]</sup> Metal nanoclusters (NCs) represent a class of sub-nanometer sized metal nanomaterials, which in many cases have a precise number of metal atoms protected with a precise number of ligands and molecule-like properties.<sup>[5]</sup> They bridge the gap between discrete atoms and plasmonic metal NPs.<sup>[5a]</sup> Their particular photo-physical properties and precise molecular formula make them different from plasmonic NPs and quantum dots. Several ultra-small NCs have already shown their potential role in a wide range of applications such as sensing, catalysis, drug delivery, imaging,<sup>[5]</sup> and even as transistors.<sup>[6]</sup>

NCs in the condensed phase was first introduced in the 1970–80s with the report of several phosphinated gold NCs such as Au<sub>11</sub>,<sup>[7]</sup> Au<sub>13</sub>,<sup>[8]</sup> Au<sub>55</sub><sup>[9]</sup> etc. The research on most of these phosphinated NCs was limited to the synthesis and characterization, except for a few assembly-related properties of Au<sub>55</sub> NCs.<sup>[10]</sup> The trend of ligands employed for the synthesis of NCs shifted towards thiolated ligands following the Brust–Schiffrin method, as thiols bind more strongly to noble metals such as Au and Ag than phosphines or other functional groups. Functionalities present on thiols can control the atomicity in NCs. For example, Au<sub>102</sub>(SR)<sub>44</sub> (R = residual group) NCs can only be synthesized through mercaptobenzoic acids.<sup>[11]</sup> This is not always true for other NCs. For instance, Au<sub>25</sub>(SR)<sub>18</sub>, or Ag<sub>44</sub>(SR)<sub>30</sub> NCs can be synthesized with a wide variety of alkyl chains R, as well as with different selenols. The physicochemical parameters employed during the synthesis procedures also allow for great control over the NCs' atomicity. Many other synthetic routes have been developed by tuning such parameters, for example, a high-temperature route,<sup>[12]</sup> carbon monoxide (CO)-directed route,<sup>[13]</sup> solid-state route,<sup>[14]</sup> ligand-exchange-induced size/structure transformation (LEIST),<sup>[15]</sup> etc. Apart from thiols, different biomolecules such as DNA, proteins, or peptides can also be utilized as protecting agents.<sup>[5a]</sup> For instance, tripeptide glutathione has been used by Whetten et al. to synthesize a series of gold NCs that were identified by laser desorption ionization mass spectrometry.<sup>[16]</sup> Later, Negishi et al. introduced polyacrylamide gel electrophoresis (PAGE) to isolate such glutathione-protected gold NCs. They characterized them through high-resolution electrospray

ionization mass spectrometry (HRESI-MS).<sup>[17]</sup> Dickson et al. worked extensively on DNA-protected, highly fluorescent silver NCs (Ag NCs).<sup>[18]</sup> Xie et al. showed for the first time that Au NCs could be made in bovine serum albumin (BSA) template without any external reducing agent.<sup>[19]</sup> Pradeep et al. developed a solid-state route to synthesize a wide variety of atomically precise Ag NCs and other metal NCs.<sup>[14,20–24]</sup> Apart from synthesis, Jin et al. devoted their work to understand the crystal structures of NCs and their structure-property relationship.<sup>[15b,25–31]</sup> many review articles are focusing on the structure, properties, and applications of metal NCs.<sup>[5,32]</sup> In this short perspective, we will highlight the mechanistic details of a few common chemical routes used in the synthesis of such atomically precise NCs. The perspective will also explain recent advancements in understanding the mechanism of NC synthesis and future challenges.

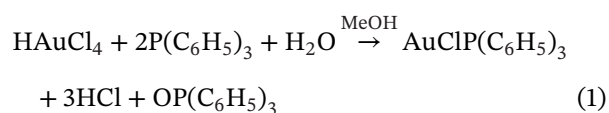
## 2 | DIFFERENT SYNTHESIS ROUTES OF NCs

As NCs, with a diameter of about 1–2 nm, fall in the size regime between atoms and NPs, two general synthetic methodologies, namely, "top-down" and "bottom-up," can be utilized for the synthesis of metal NCs (a schematic diagram is illustrated in the TOC image).<sup>[5a]</sup> In the first approach, bigger NPs or NCs are etched by employing either extra ligands<sup>[33]</sup> or by heating.<sup>[12b,34]</sup> For the latter case (second approach), metal precursors are chemically reduced in the presence of protecting ligands to synthesize NCs of specific atomicity. A wide variety of synthetic methodologies that follow the bottom-up approach have been reported, such as the Brust–Schiffrin two-phase method,<sup>[35]</sup> modifications of the Brust–Schiffrin method,<sup>[26,36]</sup> size focusing methodology,<sup>[37]</sup> CO-directed synthesis,<sup>[13]</sup> slow reduction techniques,<sup>[38]</sup> protein-mediated synthesis,<sup>[19,39]</sup> etc. In all these synthetic routes, different physico-chemical parameters of reaction conditions such as the concentration of reactants, pH and temperature of the solution, stirring speed, reducing agent, among others, play an effective role in controlling the atomicity of the synthesized NCs. In this short perspective, selected methodologies utilized to synthesize several noble metal NCs starting from classical phosphinated NCs<sup>[5a,40]</sup> to recent CO-directed synthesis<sup>[13,41]</sup> will be discussed.

### 2.1 | Classical synthetic routes: phosphinated NCs

In general, phosphinated gold NCs have been synthesized using a two-step approach. First, a gold-phosphine

complex is synthesized as a precursor, which is then chemically reduced using different reducing agents such as  $\text{NaBH}_4$ ,  $\text{B}_2\text{H}_6$ , etc. to get Au NCs of various sizes. The main disadvantage of these phosphinated NCs is their large size distribution. Contrary to phosphine ligands, diphosphine ligands are better in narrowing down the sizes of the obtained NCs.<sup>[42]</sup> The synthesis parameters such as stirring rate,<sup>[43]</sup> temperature,<sup>[44]</sup> reducing agent,<sup>[37b,45]</sup> solvents<sup>[46]</sup> etc. have a strong influence on controlling the size of the obtained NCs. Several phosphines protected gold NCs with core sizes composed of 2, 3, 4, 5, 6, 7, 8, 9, 10, 11, 13...39...55, etc. gold atoms have been successfully synthesized.<sup>[5a]</sup> For instance,  $\text{Au}_{55}(\text{PPh}_3)_{12}\text{Cl}_6$  NCs were synthesized by reduction of  $\text{AuClPPh}_3$ , which was initially synthesized by the following reaction (Equation 1);

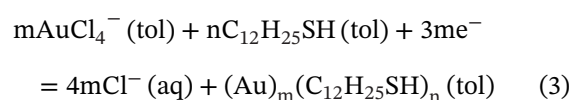
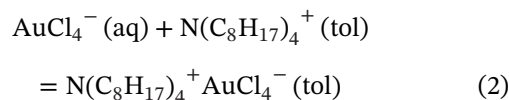


using gaseous diborane ( $\text{B}_2\text{H}_6$ ) in nonpolar solvents (e.g., benzene, toluene) at high temperature (60 °C).<sup>[9]</sup> Here,  $\text{B}_2\text{H}_6$  acts as a reducing agent, and it binds with triphenylphosphine ( $\text{PPh}_3$ ) to form a Lewis acid-base adduct ( $\text{BH}_3\text{-PPh}_3$ ), which is important to control the size of the NCs.<sup>[9,40a]</sup> However, single super-crystals of this NC have not been obtained so far. The absence of well-resolved mass spectral data and crystal structure information makes the presence of this molecule a controversial one. The initial assignment,  $[\text{Au}_{55}(\text{PPh}_3)_{12}\text{Cl}_6]$ , was proposed based on molecular weight determination and elemental analysis. The existence of several other derivatives such as  $\text{Au}_{55}[(\text{B}_{12}\text{H}_{11}\text{S})(\text{N}(\text{octyl})_4)_2]_{12}\text{Cl}_6$ ,<sup>[10]</sup>  $\text{Au}_{55}(\text{T}_8\text{-OSS-S})_{12}\text{Cl}_6$ ,<sup>[40b]</sup>  $[(\text{T}_8\text{-OSS-S} = (\text{cyclopentyl})_7\text{Si}_8\text{O}_{12}(\text{CH}_3)_2\text{S}]$ , etc., supports the proposed composition. Another way to get phosphinated NCs of specific atomicity is by conversion of other NCs. For instance,  $\text{Au}_{13}$  NCs were synthesized from  $\text{Au}_2(\text{dppm})(\text{NO}_3)_2$ .<sup>[8]</sup> Such conversion of  $\text{Au}_2$  to  $\text{Au}_{13}$  NCs can be attributed to the better structural stability, as the 13 metal atoms form a perfect icosahedron structure (one of the platonic solids).

## 2.2 | The Brust-Schiffrin method and its modifications

The synthesis direction of NCs has moved to the next level with the evolution of thiolated gold NCs due to the stronger affinity of gold atoms to sulfur than phosphorus. The preparation of thiolated monodisperse NPs in the 1980s and early 1990s has been challenging until Brust et al. introduced a two-phase method to produce narrow-sized NPs in 1994.<sup>[47]</sup> In this breakthrough method, the

metal precursor (e.g.,  $\text{HAuCl}_4$ ) was first dissolved in an aqueous solution and subsequently phase transferred to the organic phase (mainly toluene) using tetraoctylammonium bromide (TOABr). During the phase transfer, negatively charged  $\text{AuCl}_4^-$  gets exchanged with the more hydrophilic  $\text{Br}^-$ . The aqueous layer is then removed, and thiols and reducing agents are introduced into the organic phase (toluene) to obtain monodisperse NPs. Two steps are employed in the Brust method, which is, i) the phase transfer of metal precursor (Equation 2) and ii) the reduction of the phase-transferred metal ions (Equation 3).



Many reports have addressed the detailed mechanism of this synthetic methodology<sup>[48]</sup> and finding the main precursor of this reaction was a great challenge. It was initially assumed that thiol takes the leading role in reducing Au(III) to Au(I), and the Au(I)thiolate was the main precursor.<sup>[47]</sup> However, Goulet and Lennox<sup>[48a]</sup> in 2010, have shown that before the addition of borohydride, thiol solely reduces  $[\text{AuX}_4]^-$  to  $[\text{AuX}_2]^-$ , which acts as the main precursor and an Au-thiol bonding was not formed. Later, Li et al.<sup>[49]</sup> claimed that the precursor in the Brust-Schiffrin two-phase method is either a  $\text{TOA}^+[\text{AuX}_2]^-$  complex when  $[\text{RSH}]/[\text{AuX}_4]^- < 2$  or a mixture of the  $\text{TOA}^+[\text{AuX}_2]^-$  complex and the Au(I)thiolate polymer when  $[\text{RSH}]/[\text{AuX}_4]^- > 2$ . Recently, Booth et al.<sup>[48c]</sup> investigated the detailed mechanism and reaction intermediates through an electrochemical process summarized in Figure 1. They suggested that the Brust-Schiffrin two-phase method involves four steps; in the first step,  $\text{AuCl}_4^-$  ions in the aqueous phase brought into contact with tetraoctylammonium bromide ( $\text{TOA}^+\text{Br}^-$ ) present in toluene, which facilitates the gradual transfer of  $\text{AuCl}_4^-$  ions into the organic phase via an ion pair process. Then, the halide ion exchange between  $\text{AuCl}_4^-$  and  $\text{TOA}^+\text{Br}^-$  takes place in the organic layer leading to the formation of  $\text{AuBr}_4^-$ . A partial reduction of the newly formed Au(III) in the organic phase into Au(I) (i.e., from  $\text{AuBr}_4^-$  to  $\text{AuBr}_2^-$ ) is then achieved through the addition of alkanethiols (RSH). Finally, an aqueous solution of  $\text{Na}^+\text{BH}_4^-$  is added to the organic  $\text{AuBr}_2^-$  solution, whereby the  $\text{BH}_4^-$  ions brought to the organic phase by the excess  $\text{TOA}^+$  ions remain in the solution. The complete reduction of Au(I) to Au(0) occurs in the organic phase by means of  $\text{BH}_4^-$  leading to the formation of Au NPs in the organic phase.

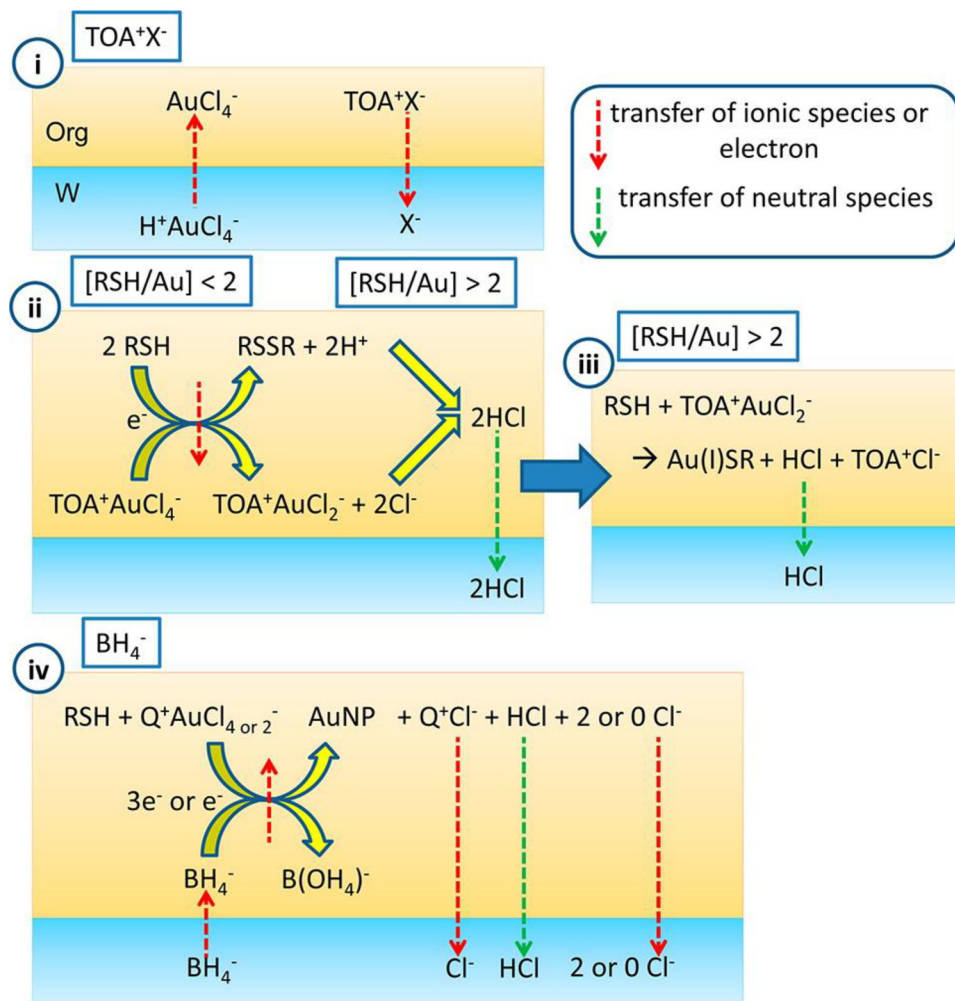


**FIGURE 1** Brust–Schiffrin’s two-phase method of NPs synthesis: In the illustration, the aqueous phase is drawn as blue and the toluene phase as yellow. Step 1 is the Au(III) phase transfer. Step 2 shows the halide ion exchange process. Step 3 shows the addition of alkanethiol, causing a reduction to Au(I). Step 4 is the phase transfer process occurring upon the addition of  $\text{NaBH}_4$ , leading to NPs formation. Taken from *ref.*,<sup>[48c]</sup> Copyright 2017 American Chemical Society

However, the proposed mechanism does not fully apply to the formation of NCs as the applied synthetic method results in polydisperse NPs from which atomically precise NCs can only be isolated via a post-synthetic treatment.

Numerous modifications of the original Brust-Schiffrin method have been developed in the last few years to obtain atomically precise NCs. For example, miscible solvents such as tetrahydrofuran (THF) were utilized to address the solubility issue of thiol and gold precursors: this method became known as the “one phase method.” Following this approach, Wu et al. synthesized  $\text{Au}_{25}(\text{SR})_{18}$  NCs.<sup>[37a]</sup> Modifications of Brust-Schiffrin methods were also made by controlling the kinetic parameters (such as stirring rate) or changing the temperature. By employing these synthetic parameter modifications, Jin et al. synthesized  $\text{Au}_{25}$  NCs.<sup>[43]</sup> Following Brust-Schiffrin’s two-phase and one-phase methods, several NCs of different atomicity were synthesized.<sup>[35b,50,51]</sup> Size focusing is another modification

strategy that has been widely applied as a post-synthetic treatment in the two-phase method to synthesize stable NCs. Chen et al.<sup>[52]</sup> showed that various magic-sized NCs could be obtained by introducing isomeric methylbenzenethiols in size focusing reaction (Figure 2). More details about size focusing strategies can be found in a review article by Jin et al.<sup>[37b]</sup>

### 2.3 | Solid-state and paste-based routes

Many synthetic routes have been dedicated to the synthesis of Au NCs. However, the synthesis of atomically precise Ag NCs was quite challenging as Ag is more prone to oxidation under aerobic conditions. In 2009, Pradeep et al. invented a new method to synthesize Ag NCs which is entirely based on a solid-state approach, and after that, the methodology has been named solid-state route.<sup>[14]</sup>



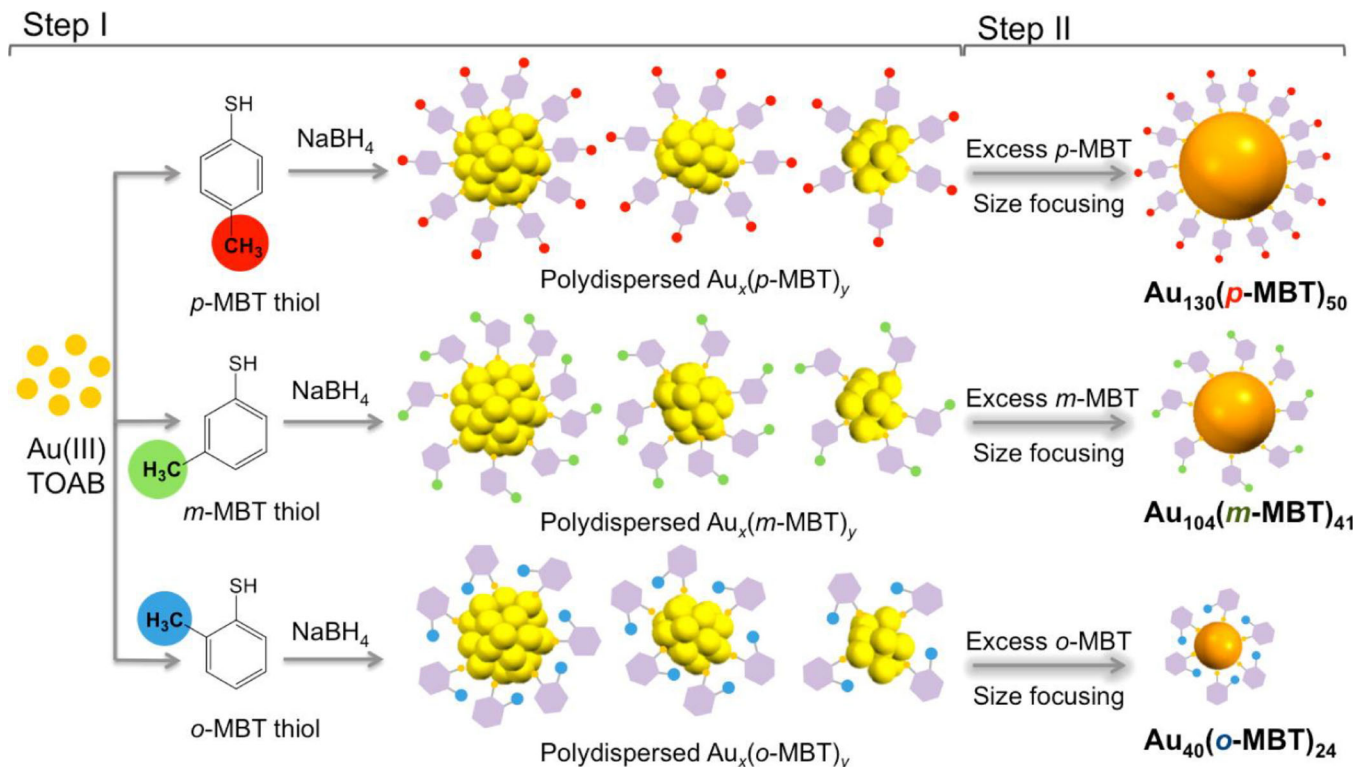


FIGURE 2 Modified Brust–Schiffrin method of NCs. Two-step size-focusing synthesis of different magic-sized nanoclusters using three isomeric thiol ligands: p-MBT, m-MBT, and o-MBT. Taken from ref.<sup>[52]</sup> Copyright 2015 American Chemical Society

In brief, it involves three steps: First, a mixture of silver nitrate (s, solid) and thiol (s) was ground in a mortar using a pestle (Figure 3). At this step the reaction took place at the interface of these two reactants due to their strong affinity to each other and polymeric thiolates were formed. Second, sodium borohydride (s) was added, and the mixture ground well, which resulted in the formation of a brownish-black powder. In the third step, water was added slowly to complete the reduction process. After that, as-synthesized NCs were purified by precipitation with ethanol and a re-extraction process. Chakraborty et al. extended the methodology using liquid thiols, which led to the discovery of many atomically precise Ag NCs.<sup>[20a,20c,20d,21,22]</sup> Using 2-phenylethanethiol (PET) as a ligand,  $\text{Ag}_{152}(\text{PET})_{60}$  can be prepared<sup>[20a]</sup> and in this case, instead of water, ethanol was added in the 3<sup>rd</sup> step, which impacted the reaction in two ways; i) controlling the size of the NCs by supplying a limited amount of water present in it, and ii) washing out the excess ligands during the centrifugation. In a similar approach, Bhattarai et al. have synthesized  $\text{Ag}_{44}(\text{SR})_{30}$  NCs starting from the thiolate-paste with 89% yield, as demonstrated in Figure 3B.<sup>[53]</sup> Unlike the solid-state route, this paste-based method offers the advantage of eliminating the exposure to volatile and hazardous ligands such as phenylethanethiol, benzenethiol, benzeneselenol, etc. Several other thiol-

stabilized NCs such as,  $\text{Ag}_9(\text{SR})_7$ ,<sup>[14]</sup>  $\text{Ag}_{44}(\text{SR})_{30}$ ,<sup>[53]</sup>  $\text{Ag}_{44}(\text{SeR})_{30}$ ,<sup>[20c]</sup>  $\text{Ag}_{55}(\text{SR})_{31}$ ,<sup>[23]</sup>  $\text{Ag}_{152}(\text{SR})_{60}$ ,<sup>[20a]</sup>  $\text{Pt}_{11}(\text{SR})_8$ ,<sup>[21]</sup>  $\text{Cu}_{38}(\text{SR})_{25}$ <sup>[20d]</sup> etc. were synthesized following the solid-state route.

## 2.4 | CO-directed route

In most of the NCs synthesis routes, sodium borohydride is used as the reducing agent. However, strong reducing agents like borohydride make it challenging to trace the intermediates formed during the synthesis of NCs. This is mainly because the reduction kinetics are much faster, and the lifetimes of many intermediates also become too short to be tracked. Slowing down the growth kinetics would be an ideal strategy to understand the mechanistic details of NCs' formation. Mild reducing agents such as sodium cyanoborohydride,<sup>[38]</sup> formic acid,<sup>[12c]</sup> etc. were used in many cases for the synthesis of NCs, but the detailed mechanism of NC growth could not be investigated. Xie et al. introduced another mild reducing agent, namely, carbon monoxide (CO), to synthesize Au NCs (Figure 4A).<sup>[13]</sup> Its reducing capability was already utilized to synthesize various noble metal NPs, especially in gold (Au) and platinum (Pt) systems.<sup>[41]</sup> The tremendous catalytic efficiency of Au in CO oxidation reactions was extensively researched and

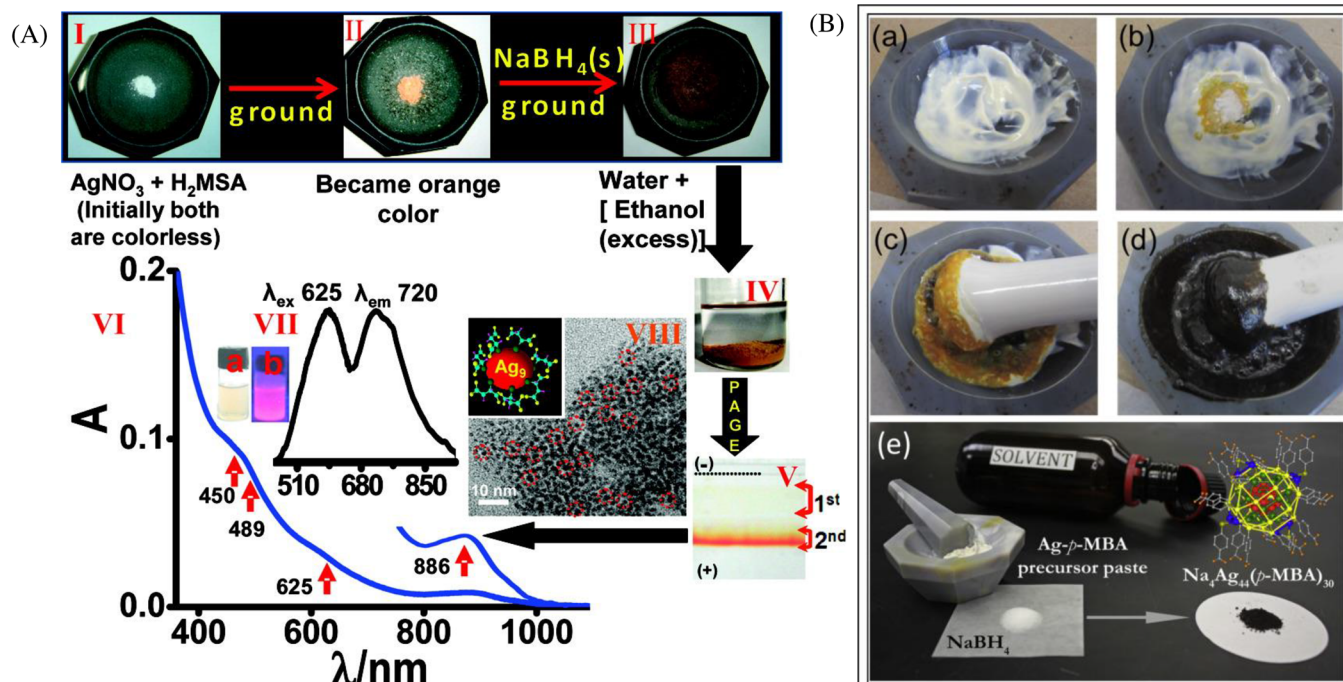


**FIGURE 3** Solid-state route of NC syntheses. A, Photographs (I-IV) representing the solid-state route to synthesize  $\text{Ag}_9(\text{SR})_7$  NCs. Other microscopic and spectroscopic characterizations are presented in V-VIII. Taken from ref.,<sup>[14]</sup> Copyright 2010 American Chemical Society. B, Step-wise synthesis of  $\text{Ag}_{44}(\text{SR})_{30}$  NCs using paste-based method originating from the “solid-state route.” Taken from ref.,<sup>[53]</sup> Copyright 2017 American Chemical Society

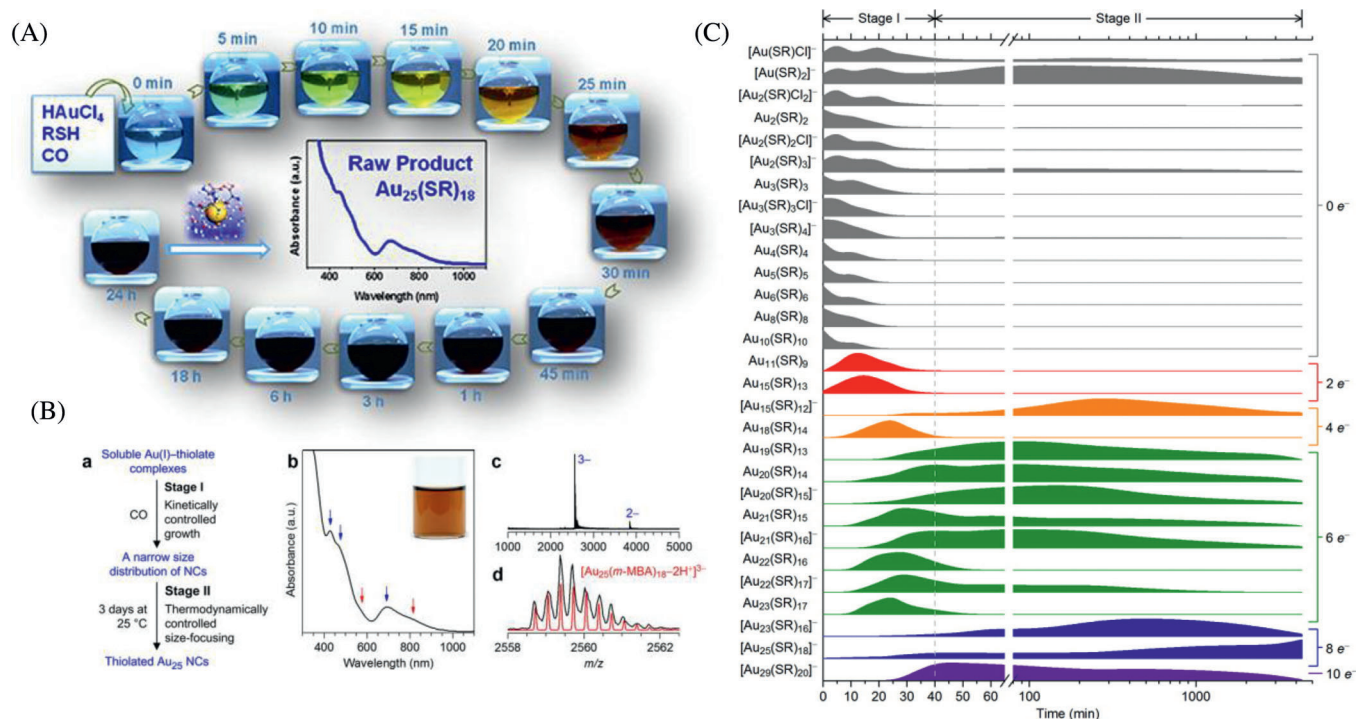
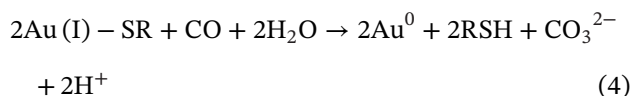


**FIGURE 4** CO-directed synthesis of NCs. A, Photographs of the  $\text{Au}_{25}(\text{SR})_{18}$  NC synthesis procedure through the CO-directed route. The inset shows the corresponding absorption spectra. Taken from ref.,<sup>[13]</sup> Copyright 2012 American Chemical Society. B, (a) Designed CO-directed synthesis of  $\text{Au}_{25}(\text{m-MBA})_{30}$  NCs. (b) UV-vis absorption and (c and d) ESI-MS spectra of NCs. C, Normalized ESI-MS spectral intensity profiles of the Au(I)-thiolate complex and NC species formed throughout the synthesis route. Taken from ref.,<sup>[54]</sup> Copyright 2014 American Chemical Society

was ascribed to the strong interaction and affinity of Au towards CO.<sup>[32]</sup> This unique interaction, which is absent in borohydride reduction routes, makes CO an important and efficient reducing agent in the synthesis of Au NCs.

Moreover, as a gaseous reducing agent, CO can quickly be released, and as a result, it has been considered a “green” reducing agent. In a typical synthesis of Au<sub>25</sub>(Cys)<sub>18</sub> NCs, aqueous HAuCl<sub>4</sub> and cysteine (Cys) solutions were mixed under vigorous stirring (Figure 4A) at basic pH.<sup>[13]</sup> Afterwards, the reaction vessel was saturated with CO, and the reaction mixture continuously monitored using spectroscopy and mass spectrometry to address the reaction mechanism and track the intermediates.

In 2014, Xie et al. probed the formation mechanism of Au<sub>25</sub>(m-MBA)<sub>18</sub> NCs synthesized through this CO-directed method, which occurs through the transformation of Au(I) complex precursors to [Au<sub>25</sub>(SR)<sub>18</sub>]<sup>-</sup> by the mild CO-mediated reduction as demonstrated in Figure 4B.<sup>[54]</sup> The Au(I)-thiolate complex precursors, as well as all the stable NC intermediates formed throughout the synthesis route, were identified (Figure 4C), and their stabilities were explained based on the number of free electrons. The kinetics of such a CO-directed route was found to be highly pH-dependent,<sup>[55]</sup> which can be easily explained from the following equation of the reduction of Au(I)-thiolate complexes by CO (Equation 4).



The reduction kinetics increase as the initial pH rises, resulting in increased atomicity of the obtained NCs.<sup>[55]</sup> With this methodology, several NCs such as Au<sub>10-12</sub>, Au<sub>15</sub>, Au<sub>18</sub>, Au<sub>22</sub>, and Au<sub>29</sub> can be synthesized by varying different reaction parameters.<sup>[55]</sup> For more information about the CO-directed synthesis route of NCs; readers are referred to a perspective article on the CO-directed route by Chen and Xie.<sup>[56]</sup>

## 2.5 | Protein-directed methods

In addition to the synthesis routes mentioned above, various bio-inspired synthetic routes have been reported to synthesize fluorescent metal NCs.<sup>[57]</sup> For instance, Xie and coworkers used BSA to synthesize red fluorescent Au NCs inspired by the naturally-occurring biomineralization process in various living organisms.<sup>[19]</sup> In their work, Xie et al. showed the capability of BSA molecules to sequester and entrap Au ions (Au<sup>3+</sup>), forming a BSA-Au(I) complex. The reaction pH was then elevated above the pK<sub>a</sub> value of their tyrosine residues (i.e., above 10), which facilitates the

reduction of the Au(I) complex in situ. Within 12 hours, highly stable Au NC@BSA composed of 25 gold atoms was subsequently formed (Figure 5A). The as-synthesized red fluorescent Au NCs showed a quantum yield (QY) around 6% and exhibited excitation and emission maxima at 480 and 640 nm, respectively. In addition to their biocompatibility, BSA endowed the Au NCs with various surface functional groups that facilitate the post-synthetic surface modification, allowing for functionalization with different surface ligands tailored for other applications.

The bioinspired work of Xie and coworkers paved the way for synthesizing other metal NCs using the BSA molecule as a reducing and protecting agent. For instance, Mathew and coworkers reported the synthesis of highly fluorescent Ag NCs composed of 15 Ag atoms confined in a BSA scaffold for the first time.<sup>[39b]</sup> Given the fact that Ag NCs are more reactive than their Au counterparts, they are more prone to self-aggregation and tend to form polydisperse NPs rendering them non-fluorescent. The confinement of such NCs in a preformed cage of BSA provides excellent stability of the as-prepared Ag NCs. In that work, Mathew et al. were able to synthesize the BSA-protected Ag<sub>15</sub> NCs that showed broad absorption features with an emission maximum at 685 nm and a fluorescence QY of 10.71%. The formation of the Ag<sub>15</sub>@BSA NCs follows the same biomineralization process mechanism involved in forming Au<sub>25</sub>@BSA NCs reported by Xie et al.,<sup>[19]</sup> where Ag ions got entrapped by BSA, which subsequently reduced at elevated pH into Ag<sub>15</sub>@BSA NCs after the addition of NaBH<sub>4</sub> (Figure 5C). Furthermore, it has been shown that by controlling the amount of added NaBH<sub>4</sub>, the emission of the NCs could be tuned from green (Ag-BSA conjugate) to red (Ag<sub>15</sub>@BSA NCs) as demonstrated in Figure 5C. Despite relatively high QY of the protein-protected NCs (~15%) compared to those of the thiol-protected NCs, it is still by far lower than those QY values reported for well-established chromophores (~95%).<sup>[58]</sup> In an attempt to synthesize protein-protected Au NCs with high QY values, Mohanty<sup>[58]</sup> and coworkers used a mixture of proteins to prepare Au NCs with a QY of 42.4%. This work illustrated that in the presence of a mixture of lysozyme (Lyz) and BSA, a BSA-Lyz adduct is formed, and Au<sup>3+</sup> ions could be reduced into Au<sup>+</sup> by the aromatic amino acid residues. The subsequent elevation of pH to 12 by adding NaOH allows for the complete reduction of Au<sup>+</sup> into Au<sup>0</sup> NCs within 12 hours (Figure 5B). Mohanty et al. showed that under such reaction conditions, Au NCs could be either formed inside the BSA molecule. Then Lyz tends to form an aggregate with the BSA-protected Au<sub>36</sub> NCs, or the NCs formed freely in the solution and then got protected by both proteins.<sup>[58]</sup>

The mixed protein-protected Au NCs (~Au<sub>36</sub>@BSA-Lyz) showed high QY values (~42.4%) and exhibited 3- to



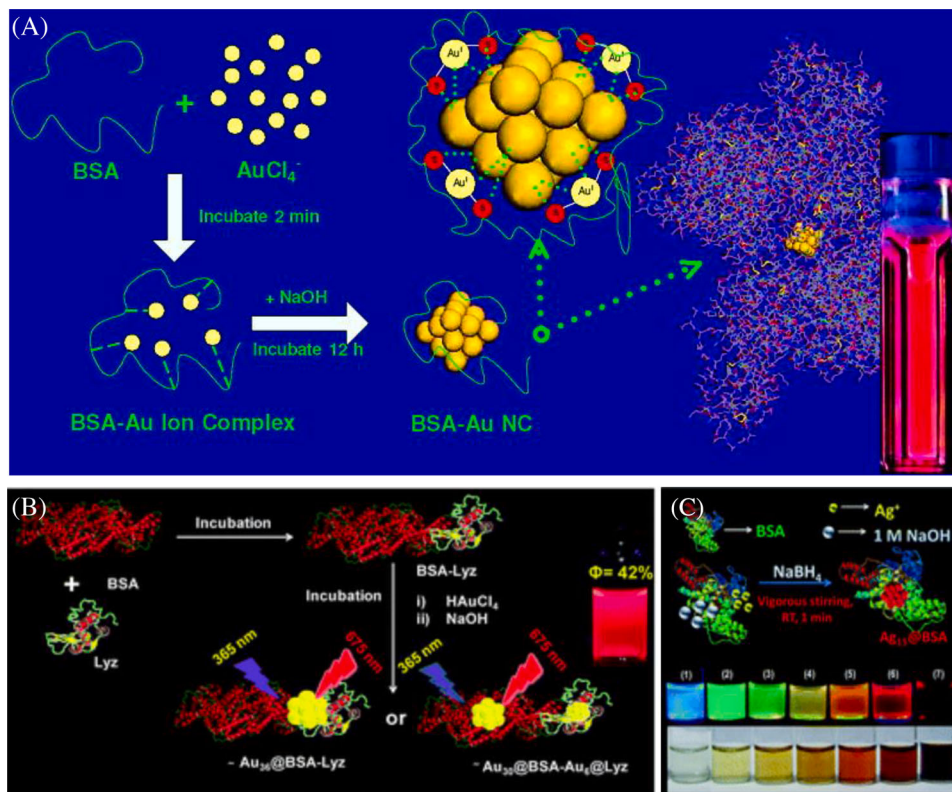


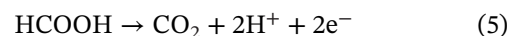
**FIGURE 5** Protein-directed route of NC synthesis. A, Protein directed synthesis of fluorescent Au NCs using BSA. Taken from ref.,<sup>[19]</sup> Copyright 2009 American Chemical Society. B, Synthesis of highly fluorescent Au NCs using a mixture of Lysozyme and BSA. Taken from ref.,<sup>[58]</sup> Copyright 2015 The Royal Society of Chemistry. C, Synthesis of Ag NCs with tunable fluorescence using BSA. Taken from ref.,<sup>[39b]</sup> Copyright 2011 The Royal Society of Chemistry

the 4-fold enhancement of the fluorescence intensity compared to NCs prepared using individual proteins, namely,  $\sim\text{Au}_{30}@BSA$  and  $\text{Au}_{10}@Lyz$ , respectively.<sup>[58]</sup> This apparent increase in the fluorescence intensity is attributed to the inter-protein Förster resonance energy transfer (FRET) process between the FRET donor (protein mixture) and the FRET acceptor (Au NCs); this phenomenon is supported by the proximity of BSA and Lyz to each other around the Au NCs core.

## 2.6 | High-temperature routes

Although the formation of various metallic NCs at relatively high temperatures has been shown to proceed through an etching process of the preformed NPs (top-down method),<sup>[12a,12b]</sup> the direct synthesis of atomically precise NCs starting from their metallic salts (bottom-up technique) is challenging as their synthesis is quite sensitive (the growth kinetics of NCs is much faster at elevated temperature) and usually takes place in low-temperature conditions. In 2012, Chakraborty and coworkers<sup>[12c]</sup> reported for the first time the synthesis of glutathione (GSH)-protected Ag NCs using a high-

temperature synthesis route. In this work, the reducing power of formic acid was activated at 70°C, which thereby became capable of reducing Ag ions into  $\text{Ag}^0$ , giving rise to glutathione-protected Ag NCs (Figure 6A). The reaction completed within 3 hours and the as-synthesized ultra-small red-fluorescent NCs (0.85 nm) were shown to be composed of 75 Ag atoms protected by 40 glutathione ligands ( $\sim\text{Ag}_{75}(\text{SG})_{40}$ ) and exhibited excitation maxima at 360, 400 and 430 nm as well as an emission maximum at 670 nm. The occurring decomposition of formic acid at high temperature was believed to proceed via the following reaction (Equation 5):



The pH of the mixture changes from 5.8 to 2.4 during the course of the reaction, which validates the above decomposition mechanism. Zheng and coworkers<sup>[12d]</sup> also reported the synthesis of ultra-stable and fluorescent Ag NCs through a similar high-temperature synthesis route. They showed that the delicate control of the Ag NCs' structure could enhance their QY as well as their stability in aqueous solution, which is of great importance for Ag NCs due to their susceptibility to oxidation



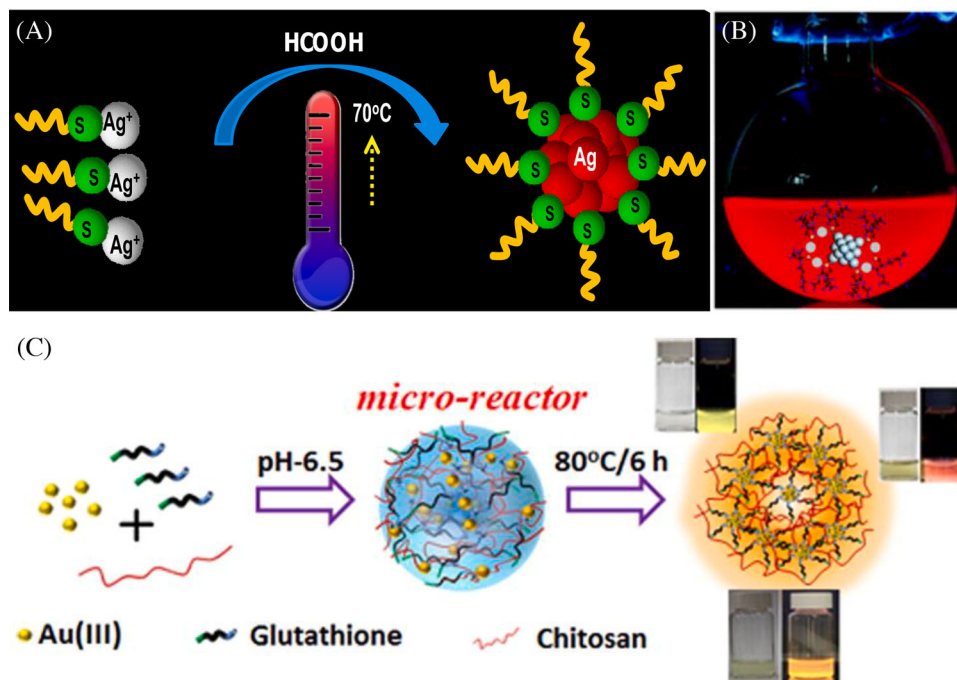


**FIGURE 6** High-temperature assisted synthesis of NCs. A, synthesis of glutathione-protected Ag NCs. Taken from ref.,<sup>[12c]</sup> Copyright 2012 The Royal Society of Chemistry. B, Large-scale synthesis of Ag NCs using the high-temperature protocol. Taken from ref.,<sup>[12d]</sup> Copyright 2015 The Royal Society of Chemistry. C, Spatially confined synthesis of Au NCs within the nanogel microreactor through the heat-assisted route. Taken from ref.,<sup>[61]</sup> Copyright 2016 American Chemical Society

in aqueous media.<sup>[59]</sup> The high-temperature route overcomes the energy barrier of the redox reaction of Ag(I)/Ag(0) and thereby facilitates the reduction of Ag (I) ions into Ag (0) core atoms driven and protected by GSH. Furthermore, the elevated temperature is crucial for thiol etching (NC digestion process) as well as the condensation of the Ag(I)-thiolate complexes on the surface of the in situ formed NCs.<sup>[12d]</sup> These Ag(I)-thiolate complexes form a shell around the NCs core and are responsible for the oxidation resistance as well as the thermodynamic stability of the as-synthesized Ag NCs. Moreover, the high-temperature route offers large-scale synthesis of high-quality Ag NCs in a single batch (Figure 6B). The as-synthesized red-fluorescent Ag(0)@Ag(I)-thiolate core-shell NCs are  $\leq 2$  nm in size and exhibit a featureless UV-vis absorption spectrum. Zheng and coworkers suggested that this featureless spectrum is similar to the aggregation-induced emission (AIE) in Au NCs. The origin of fluorescence of such Ag NCs is majorly due to the AIE of the Ag(I)-thiolate complexes on the surfaces of the in situ generated Ag(0) cores. The oxidation state was verified by X-ray photoelectron spectroscopy (XPS), which showed that the predominant species of the as-synthesized Ag NC is the Ag(I) (~54%). This is in agreement with the high oxidation state feature exhibited by AIE-type NCs due to the high metal(I)-thiolate proportion of such NCs.<sup>[12d]</sup> Furthermore, the Ag NCs were shown

to be a mixture of three different NC species, namely Ag<sub>10</sub>SG<sub>5</sub>, Ag<sub>10</sub>SG<sub>6</sub> and Ag<sub>11</sub>SG<sub>7</sub>.

Many attempts have been made to enhance the fluorescence of metal NCs, however most of those strategies result in non-biocompatible NCs (due to ligands or solvents), and hence they are not suitable for the biomedical applications.<sup>[60]</sup> In an attempt to address this issue, Goswami and coworkers<sup>[61]</sup> reported the synthesis of highly fluorescent Au NCs via the high-temperature route spatially confined in biocompatible polymeric nanogel matrix. The Au NCs reported in this study take the advantage of both, the highly fluorescent NCs synthesized by the high temperature protocol as well as the large surface area, biocompatibility, multifunctionality, and stimuli-responsiveness of the nanogel. Under specific pH conditions, an electrostatic interaction between the negatively-charged COO<sup>-</sup> groups of the Au(I)-SG complex (GSH used as the thiolate ligand) and the positively-charged H<sub>3</sub>N<sup>+</sup> of the water-soluble polymer chitosan makes the subsequent self-assembly of the complex resulting in formation of nanogel. Then, the Au(I)-thiolate complexes are spatially confined within this nanogel microreactor, a process that facilitates the rapid formation (only 6 hours, in comparison to 24 hours without using the polymeric chitosan) of highly fluorescent Au(0)@Au(I)-thiolate core-shell NCs (Figure 6C). The as-synthesized orange-fluorescent Au(0)@Au(I)-SG NCs are

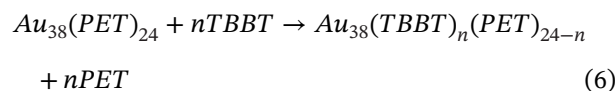
$\sim 1.03 \pm 0.52$  nm in size and exhibit excitation and emission maxima at 375 nm and 615 nm, respectively.<sup>[61]</sup> This high temperature microreactor-facilitated route of NC formation offers large-scale production of high-quality Au NCs. Furthermore, the enhancement of the fluorescence of such NCs was ascribed to the strong coordinative bonds between the  $\text{COO}^-$  groups of the Au(I)-SG complex and the  $\text{H}_3\text{N}^+$  of the chitosan rigidifying the Au(I)-thiolate shell and in turn prohibiting the relaxation of the excited NCs as well as the nonradiative decay processes. Goswami and colleagues therefore ascribed such an enhancement in the fluorescence of the as-prepared NCs to a matrix-coordinate-induced aggregation effect.<sup>[61]</sup>

## 2.7 | Ligand-exchange-induced size/structure transformation (LEIST)

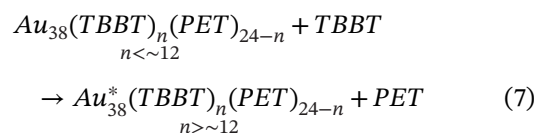
Since atomic precision and molecular purity are desirable physicochemical properties in many fundamental studies and many promising applications,<sup>[62]</sup> substantial research efforts have been devoted to controlling the atomic precision of NPs/NCs over the last two decades.<sup>[63]</sup> One of the widely established methodologies to achieve atomic precision and molecular purity in nanochemistry is the size focusing technique, which involves two steps, the kinetically controlled synthesis of different-sized  $\text{Au}_n(\text{SR})_m$  NCs with various stability properties, followed by the thermodynamically driven ligand-induced size-focusing/conversion process of the NCs mixture into a single mostly-stable NC.<sup>[37b,64]</sup> However, these techniques vary somehow in their outcomes. Usually, they involve complex interdependent variables that make control over NC's size and structure quite challenging. Recently, ligand-exchange, which may be either partial or full and usually associated with NC core size change, has provided a new tool for the post-synthetic fine control of NCs to obtain a desired size/structure. For instance, Bootharaju and coworkers<sup>[15a]</sup> were able to post-synthetically convert the  $\text{Ag}_{35}(\text{GSH})_{18}$  NCs into  $\text{Ag}_{44}(4\text{-fluorothiophenol})_{30}$ , taking advantage of the ligand-exchange-induced resizing capability in an immiscible biphasic liquid system at room temperature. This study has also shown that different NC sizes other than the  $\text{Ag}_{44}(4\text{-fluorothiophenol})_{30}$  could be obtained by rationally selecting the incoming thiolated ligand during the ligand-exchange (LE) process of  $\text{Ag}_{35}(\text{GSH})_{18}$  (Figure 7B). Furthermore, Bootharaju et al. showed that not only the LE process was able to convert  $\text{Ag}_{35}(\text{GSH})_{18}$  into the larger  $\text{Ag}_{44}(4\text{-fluorothiophenol})_{30}$  NCs but also was able to facilitate the reverse reaction and convert the later NCs into the original  $\text{Ag}_{35}(\text{GSH})_{18}$  NCs with a 50% yield (Figure 7B). It is worth noting that the reverse reaction involves a size focusing step resulting in

a mixture of  $\text{Ag}_{35}(\text{GSH})_{18}$ ,  $\text{Ag}_{37}(\text{GSH})_{21}$ , and  $\text{Ag}_{36}(\text{GSH})_{20}$  NCs, which finally are converged to  $\text{Ag}_{35}(\text{GSH})_{18}$  NCs. While the LE forward reaction of  $\text{Ag}_{35}$  NCs to  $\text{Ag}_{44}$  NCs proceeds very fast in a one-step process, the reverse reaction of the LE process occurs slowly. It involves converting the metastable NCs into single NC type via a thermodynamically-driven mass transfer mechanism from one NC to the other.

In 2012, Zeng and coworkers<sup>[15b]</sup> also reported using LE-induced NC size and structure transformation (LEIST) to obtain different new Au NCs. In their work, they showed the successful thiol-for-thiol thermal LE of pure  $\text{Au}_{38}(\text{PET})_{24}$  NCs (PET =  $\text{SC}_2\text{H}_4\text{Ph}$ ) with 4-tert-butylbenzenethiol (TBBT) resulting in a shrinkage of the original NCs size to  $\text{Au}_{36}(\text{TBBT})_{24}$  (Figure 7A). This process assists the high yield production of pure  $\text{Au}_{36}(\text{TBBT})_{24}$  (> 90 %), which in turn facilitates the crystallization of the LE product revealing their unusual FCC crystal structure. To this end, the  $\text{Au}_{36}(\text{TBBT})_{24}$  NC was the first to exhibit FCC kernel structure in the  $\text{Au}_n(\text{SR})_m$  NC family. In 2013, Zeng and coworkers<sup>[65]</sup> showed that the LEIST process of  $\text{Au}_{38}(\text{PET})_{24}$  to  $\text{Au}_{36}(\text{TBBT})_{24}$  involves four stages (Figure 7A). **Stage I:** during which partial LE takes place without any alteration in size, structure, or optical features of the original NCs, giving rise to a mixed-ligand  $\text{Au}_{38}(\text{TBBT})_n(\text{PET})_{24-n}$ , where  $n < \sim 12$  (Equation 6).



**Stage II:** as time proceeds further, LE, as well as TBBT incorporation on the NCs surface, takes place, which in turn induces structural distortion of the original  $\text{Au}_{38}$  NC ( $\text{Au}_{38}^*$  in the following equation denotes the distorted structure), to accommodate more bulky TBBT, accompanied by changes in their UV-vis spectral features (Equation 7).



**Stage III:** during this stage, disproportionation reaction takes place whereby the two released Au atoms from  $\text{Au}_{38}(\text{SR})_{24}$  during the size transformation/internal reconstruction into  $\text{Au}_{36}(\text{SR})_{24}$  are captured by another  $\text{Au}_{38}(\text{SR})_{24}$  and giving rise to  $\text{Au}_{40}(\text{SR})_{26}$ , note that two more TBBT ligands are incorporated into the newly formed NCs. As reaction proceeds, the proportions of  $\text{Au}_{36}$  and  $\text{Au}_{40}$  increase, whereas the proportion of  $\text{Au}_{38}$  decreases (Equation 8).

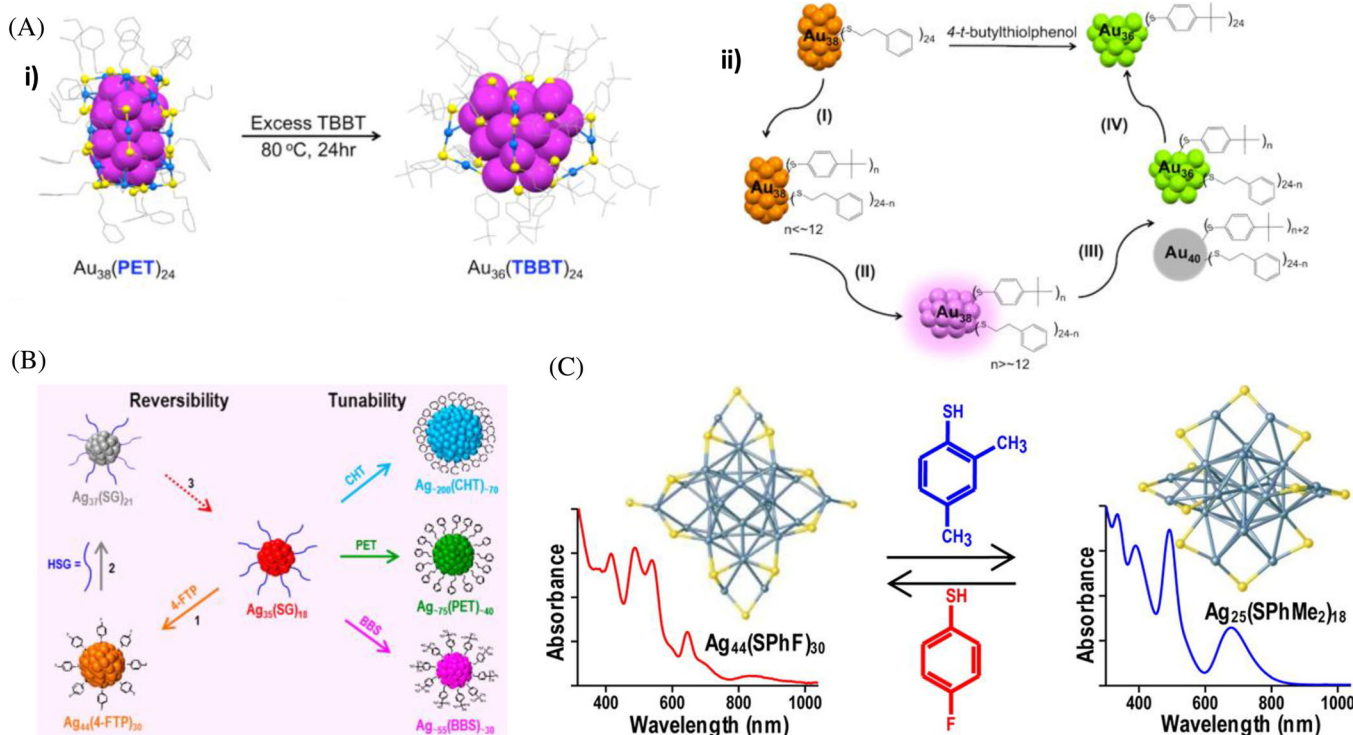
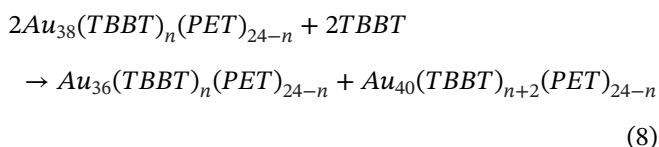
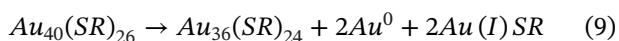


**FIGURE 7** Ligand-exchange-induced size and structure transformation of NCs. A(i), Synthesis of  $Au_{36}(TBBT)_{24}$  through ligand-exchange of  $Au_{38}(PET)_{24}$  with TBBT at high temperature. Taken from ref.,<sup>[67]</sup> Copyright 2015 American Chemical Society. A (ii), Different stages involved in the ligand-exchange-induced size and structure transformation of  $Au_{38}(PET)_{24}$  into  $Au_{36}(TBBT)_{24}$ . Taken from ref.,<sup>[65]</sup> Copyright 2013 American Chemical Society. B, reversibility and tunability of the ligand-exchange-induced size/structure transformation route. Taken from ref.,<sup>[15a]</sup> Copyright 2015 American Chemical Society. C, forward and reverse reactions of the ligand-exchange-induced size/structure transformation of  $Ag_{44}(SPhF)_{30}$  NCs. Taken from ref.,<sup>[66]</sup> Copyright 2016 American Chemical Society



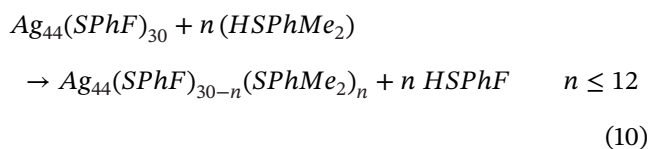
**Stage IV:** after the completion of the disproportionation reaction, a temperature-driven conversion of the remained  $Au_{40}(SR)_{26}$  to  $Au_{36}(SR)_{24}$  takes place (Equation 9) as well as the excess TBBT-driven size focusing, which is accompanied by the high-yield formation of molecularly pure  $Au_{36}(SR)_{24}$ .



Despite the efficiency of the biphasic LE process in the high-yield synthesis routes of molecularly pure NCs, the underlying NCs resizing/restructuring mechanisms induced by such routes remain unrevealed due to the abrupt chemical transformation of the NCs, as well as the biphasic nature usually encountered during the biphasic LE process.<sup>[66]</sup> To address such limitations,

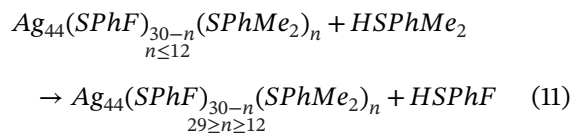
Bootharaju and coworkers<sup>[66]</sup> designed a slow monophasic LE reaction to track the structural transformation of hollow  $Ag_{44}(SPhF)_{30}$  NCs (SPhF: 4-fluorobenzenethiolate) into the non-hollow  $Ag_{25}(SPhMe_2)_{18}$  NCs (SPhMe<sub>2</sub>: 2,4-dimethylbenzenethiolate) and vice versa (Figure 7C). The LE pathway follows four stages which are quite similar to the above mentioned four stages reported by Zeng et al.<sup>[65]</sup>

In the first stage (**Stage I, partial LE**), 18 of the incoming SPhMe<sub>2</sub> ligands replace 18 of the SPhF ligands on the surface of  $Ag_{44}(SPhF)_{30}$  NCs producing  $Ag_{44}(SPhF)_{12}(SPhMe_2)_{18}$  as the predominant LE product. Other intermediate species have also been observed but in low proportions. After 1 hour of the LE reaction, equal proportions of  $Ag_{44}(SPhF)_{12}(SPhMe_2)_{18}$  and  $Ag_{44}(SPhF)_1(SPhMe_2)_{29}$  coexist in the reaction mixture as the predominant products (Equation 10).

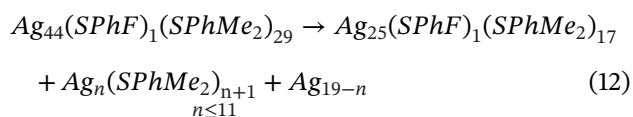




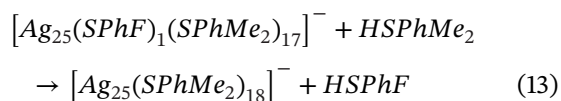
**(Stage II, nearly complete LE):** after 2 hours of the reaction, the  $\text{Ag}_{44}(\text{SPhF})_1(\text{SPhMe}_2)_{29}$  predominates (Equation 11), which in turn induces structural distortion of the original NCs driven by the increased steric hindrance between the incoming bulky ligands.



**(Stage III, disproportionation):** during which the disproportionational dissociation of  $\text{Ag}_{44}(\text{SPhF})_1(\text{SPhMe}_2)_{29}$  into  $\text{Ag}_{25}(\text{SPhF})_1(\text{SPhMe}_2)_{17}$  accompanied by the release of  $\text{Ag}_n(\text{SPhMe}_2)_{n+1} + \text{Ag}_{19-n}$ , where  $n \leq 11$  (Equation 12). The released fragments may be uptaken by the remaining  $\text{Ag}_{44}(\text{SPhF})_1(\text{SPhMe}_2)_{29}$ , giving rise to a mixture of metastable larger intermediates such as  $[\text{Ag}_{46}(\text{SPhF})_9(\text{SPhMe}_2)_{21}]^{2-}$ ,  $[\text{Ag}_{48}(\text{SPhF})_7(\text{SPhMe}_2)_{23}]^{2-}$ , and  $[\text{Ag}_{50}(\text{SPhF})_4(\text{SPhMe}_2)_{26}]^{2-}$ .



**(Stage IV, size focusing):** after 3–4 hours, the metastable intermediates decomposed into  $\text{Ag}_{25}(\text{SPhF})_1(\text{SPhMe}_2)_{17}$  driven by the size focusing process. Since  $\text{HSPhMe}_2$  ligands are present in excess in the reaction mixture, the  $\text{Ag}_{25}(\text{SPhF})_1(\text{SPhMe}_2)_{17}$  NCs are ultimately transformed into the molecularly pure  $[\text{Ag}_{25}(\text{SPhMe}_2)_{18}]^{-1}$  NCs (Equation 13) with a high yield (~80%).



Furthermore, it has been shown that the reverse reaction also involves four stages and occurs relatively fast compared to the forward reaction, and the  $\text{SPhMe}_2$  of the  $\text{Ag}_{25}(\text{SPhMe}_2)_{18}$  could be rapidly replaced with  $\text{HSPhF}$  within 1 hour. The reverse reaction's transformation process involves the dimerization of the mixed ligand  $\text{Ag}_{25}$  NCs into metastable  $\text{Ag}_{50}$  intermediates, which undergo a set of disproportionation reactions giving rise ultimately to the  $[\text{Ag}_{44}(\text{SPhF})_{30}]^{4-}$  NCs. This study showed that the chemical composition of the ligands, such as their electron-donating/withdrawing capabilities as well as the bulkiness of such ligands are predicted to play a crucial role in determining the size and structure of the obtained NCs during the LE process.

## 2.8 | Combination of both bottom-up and top-down (CBBT) method

Although most of the NCs' synthetic methodologies involve either bottom-up or top-down techniques, both might also take place in a single synthetic route. For instance, Adhikari and Banerjee<sup>[68]</sup> reported in 2010 the synthesis of fluorescent Ag NCs using the reduced form of lipoic acid (dihydrolipoic acid, DHLA) as a ligand via bottom-up and top-down routes. Later, in 2012, Muhammed and coworkers have explained the growth process of such fluorescent AgNCs through a kinetic model.<sup>[69]</sup> In our recent report,<sup>[70]</sup> different stages of the formation mechanism of such DHLA-protected Ag NCs are explained step by step (Figure 8A-B). In this study, we illustrated that the synthesis pathway of the  $\text{Ag}_{29}(\text{DHLA})_{12}$  NCs, which were first reported by Adhikari and Banerjee,<sup>[68]</sup> can be divided into four stages. **Stage I** involves reducing the lipoic acid into its reduced dihydrolipoic acid form via  $\text{NaBH}_4$ -induced breakage of the disulphide bonds. **Stage II:** shortly after the addition of the  $\text{AgNO}_3$  to the reaction mixture which contains DHLA, the DHLA coordinates with the Ag(I), and subsequently, the Ag(I)-thiolate is formed, followed by **Step III:** during which the formation of the bigger Ag NPs (bottom-up route) takes place as became evident from the UV-Vis absorption spectra as well as the dynamic light scattering (DLS) data of the aliquots taken at this stage. **Stage IV:** during which the formed Ag NPs are subjected to consecutive core-etching and size focusing processes induced by surface ligands (top-down route) until reaching the most thermodynamically stable Ag NC, which is  $\text{Ag}_{29}(\text{DHLA})_{12}$  NCs. The as-synthesized red-fluorescent Ag NCs showed the characteristic molecule-like UV-Vis absorption features of  $\text{Ag}_{29}(\text{DHLA})_{12}$  NCs and exhibited excitation and emission maxima ~425 nm and ~650 nm, respectively. The HR-TEM images of the  $\text{Ag}_{29}(\text{DHLA})_{12}$  NCs showed that they are 2.44 nm in size and revealed no larger NPs nor any form of aggregation.<sup>[68]</sup>

The nucleation and growth of these  $\text{Ag}_{29}$  NCs were demonstrated by van der Linden and coworkers<sup>[71]</sup> through mass spectrometry and X-ray absorption spectroscopy (XAS) studies. Since the initial growth and nucleation involved the formation of larger NPs, a mass spectrometric analysis was not successful in capturing the details of the first half, which is a bottom-up process. Still, it was assumed that such NPs contain more than hundreds of Ag atoms. In the second stage, during the top-down method, the evolution of  $\text{Ag}_{29}$  NCs occurred via  $\text{Ag}_{28}$  and  $\text{Ag}_{26}$  NCs, as suggested by the mass spectrometry data (Figure 8C). The remarkable stability of  $\text{Ag}_{29}$  NCs ( $8e^-$  system, a close shell electronic structure) is the

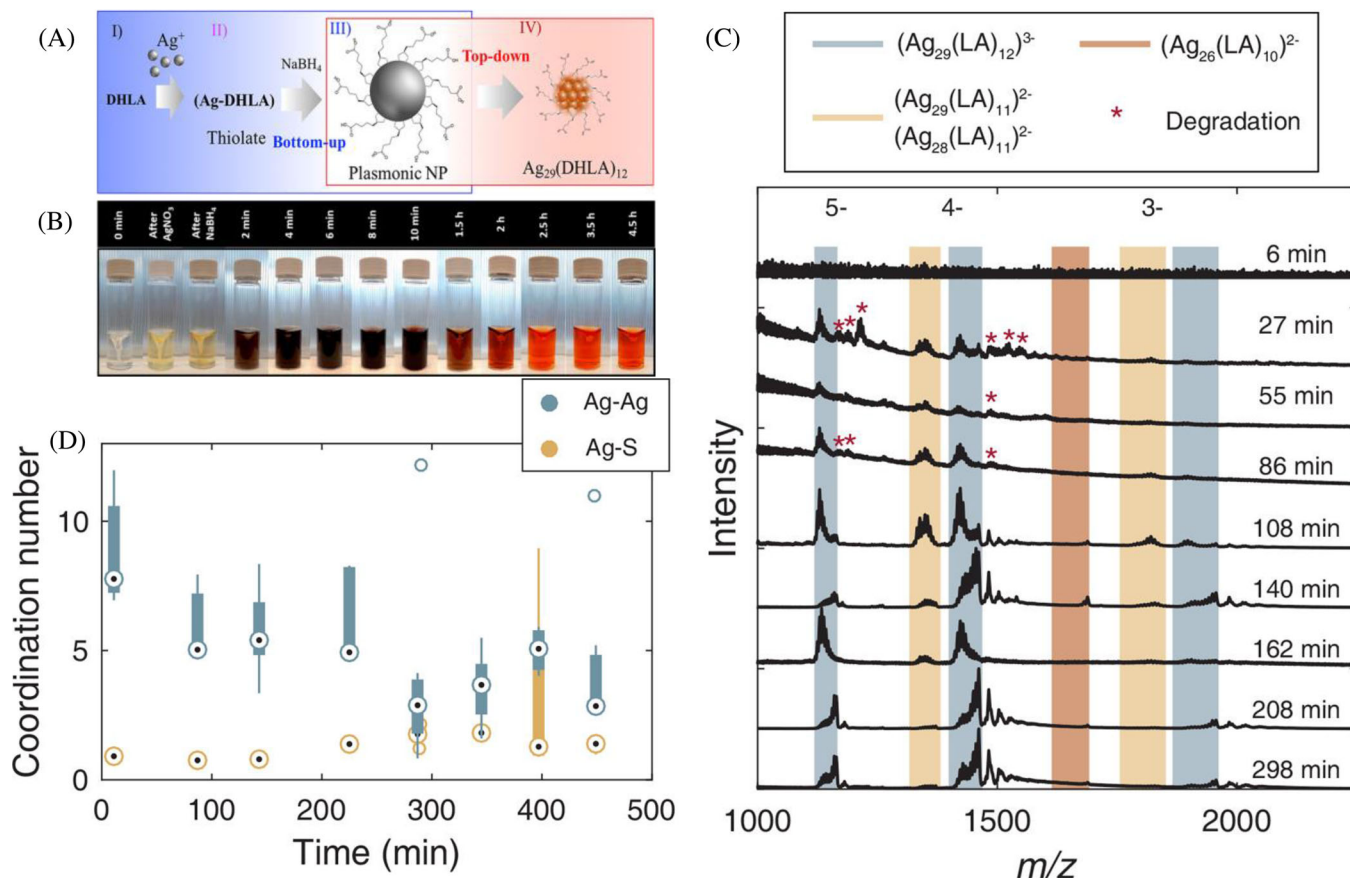


**FIGURE 8** Combination of bottom-up and top-down methodologies. A, different stages involved in the synthesis of  $\text{Ag}_{29}(\text{DHLA})_{12}$  NCs by the bottom-up and top-down routes. B, photographs show the evolution of the  $\text{Ag}_{29}(\text{DHLA})_{12}$  NCs over time. Taken from ref.,<sup>[70]</sup> Copyright 2019 American Chemical Society and Division of Chemical Education, Inc. C, Mass spectra of Ag NCs at various times after  $\text{NaBH}_4$  addition. The ion signals of  $(\text{Ag}_{29}(\text{LA})_{12})^{3-}$  are marked in blue; those of the other observed clusters in red and yellow. D, Ag–Ag and Ag–S coordination numbers determined from EXAFS data during the synthesis of  $\text{Ag}_{29}$  NCs, shown as box plots. Taken from ref.,<sup>[71]</sup> Copyright 2018 American Chemical Society

major driving force for this two-step synthesis. Extended time-dependent information about coordination numbers generated from X-ray absorption fine structure (EXAFS) data (Figure 8D) shows the decrease in Ag–Ag and increase in Ag–S coordination number over time, supporting the two-step mechanism.

### 3 | SUMMARY AND FUTURE PERSPECTIVES

Despite the excessive reports on the synthesis of noble metal NCs, the detailed crystal structure has been only solved for a few limited NCs, though. Structural analysis of metal NCs can address many fundamental questions on the origin of their unique properties. Therefore, the crystallization of NCs is one of the major perspectives that need to be pursued to unravel their in-depth-chemistry. The purity and stability of NCs are found to be the most critical issues for the crystallization process. Currently, there are many

reported approaches through which both the purity and the stability of NCs can be improved, which will be discussed below.

Most of the highlighted synthesis approaches mentioned above, including the size-focusing and LEIST methodologies, imply the reaction of a strongly binding molecule with the in situ formed or existing noble metal NCs. Thereby, molecules with a robust noble-metal-sulfur bond, for example,  $[\text{Au}_2(\text{TPP})_2(\text{SC}_2\text{H}_4\text{Ph})]^+$  complexes, are formed during the synthesis of  $[\text{Au}_{25}(\text{TPP})_{10}(\text{SC}_2\text{H}_4\text{Ph})_5\text{Cl}_2]^{2+}$  NCs and released into the solution.<sup>[72]</sup> Other undesired inorganic residues are large polydisperse NPs and are either formed during the synthesis<sup>[73]</sup> or present as the unreacted starting material in a size-focusing approach. Moreover, the size-determining organic ligands are prone to side reactions with oxygen and other radicals,<sup>[74]</sup> resulting in, for example, TPP-oxide formation<sup>[75]</sup> for the case of  $[\text{Au}_{25}(\text{TPP})_{10}(\text{PET})_5\text{X}_2]^{2+}$  ( $\text{X} = \text{Cl}$  or  $\text{Br}$ ) NCs synthesis and as their chemical structure is altered thereby resulting

in additional byproducts to be removed after the NC synthesis.

Several purification strategies were investigated and applied to the as-synthesized NCs. These include simple approaches as there are extraction/precipitation or filtration<sup>[73,75,76]</sup> as well as instrument-supported separation techniques, such as high-performance liquid chromatography (HPLC)<sup>[76]</sup> or PAGE.<sup>[16]</sup> These instrument-based methods were initially used to separate NCs with a narrow size distribution from a polydisperse ensemble.<sup>[77]</sup> However, as the synthesis strategies for noble metal NCs advanced which allowed for discrete NC sizes to be synthesized, the application possibilities have also widened, for instance, high-resolution separation of NCs from ligand exchange or doping reactions,<sup>[78]</sup> with various atomically precise sizes, ligand compositions, coordination isomers, and charge states became feasible.<sup>[78,79]</sup> Many other separation techniques such as thin-layer chromatography,<sup>[80]</sup> size exclusion chromatography,<sup>[81]</sup> or even analytical ultracentrifuge<sup>[82]</sup> have been employed in the purification process various NCs.

Despite the significant advances in HPLC, a thorough purification evidenced by a combination of MS, <sup>1</sup>H-, <sup>31</sup>P-NMR was targeted only in a limited number of publications.<sup>[50c,83]</sup> Most striking though is the missing low *m/z* region in the mass spectra of NCs.<sup>[73,84–86]</sup> This is, however, exactly the region where signals of small inorganic byproducts such as Au<sub>2</sub>TPP<sub>2</sub>PET, Au<sub>2</sub>(SR)<sub>3</sub>, Au(SR)<sub>3</sub>, Ag(SR)<sub>3</sub>, Ag<sub>2</sub>(SR)<sub>5</sub> et.c. can be seen.

The most commonly used purification strategy for freshly synthesized atomically precise noble metal NCs is to wash agglomerates with more polar and nonpolar anti-solvents.<sup>[78]</sup> This approach is utilized in Au NC systems with core sizes ranging from Au<sub>11</sub> to Au<sub>333</sub>. It aims to remove the unbound ligand molecules,<sup>[64c,73]</sup> phase transfer agents as the tetraoctylammonium ion, small NCs, and large polydisperse NPs. However, the success of such washing procedures is highly dependent on the solubility of NCs, which is impacted by the hydrophilicity of the surface-bound ligands and their charge state, as in the case of organic-soluble NCs. This becomes evident from residual signals of tetraoctylammonium ions present in the NMR-spectrum of [Au<sub>25</sub>(TPP)<sub>10</sub>(PET)<sub>5</sub>]<sup>2+</sup> or of [Au<sub>25</sub>(PET)<sub>18</sub>]<sup>1-</sup> and their absence in that of [Au<sub>25</sub>(PET)<sub>18</sub>]<sup>0</sup> NCs.<sup>[33b,87]</sup>

Collectively, it becomes evident from the versatility of the employed molecules in NC syntheses; real purity can only be achieved with a combination of analytical techniques. The importance of post-synthetic removal of these residual molecules is as critical as challenging for various reasons: the electronic and chemical properties of NCs and their inorganic byproducts are similar as their size only differs by several inorganic atoms and ligand molecules, potentially resulting in undesired

interference on the applications level. They can play a significant role in quenching of catalytic activity or catalyst poisoning,<sup>[88]</sup> or undesirably bio-conjugated to a target instead of the NCs,<sup>[89]</sup> or quenching the NCs' fluorescence by a charge-transfer, or affect the charge transport in NC based thin films.<sup>[6]</sup> So, such impurities are becoming a big burden in pertaining novel applications of these atomically precise NCs and improved purification strategies need to be implemented for better applicability as well as structure-property correlation.


## ACKNOWLEDGMENT

Mustafa Gharib acknowledges the Ministry of Higher Education and Scientific Research (MHESR) of Egypt and the Deutscher Akademischer Austauschdienst (DAAD) for his fellowship. I. C. thanks Fonds der Chemischen Industrie im Verband der Chemischen Industrie for support. This work was supported by the Cluster of Excellence "Advanced Imaging of Matter" of the Deutsche Forschungsgemeinschaft (DFG) - EXC 2056 - project ID 390715994.

## CONFLICT OF INTEREST

The authors declare no conflict of interest.

## ORCID

Wolfgang J. Parak  <https://orcid.org/0000-0003-1672-6650>

Indranath Chakraborty  <https://orcid.org/0000-0003-4195-9384>

## REFERENCES

1. a) L. Yang, Z. Zhou, J. Song, X. Chen, *Chem. Soc. Rev.* **2019**, *48*, 5140; b) Y. Chen, Z. Fan, Z. Zhang, W. Niu, C. Li, N. Yang, B. Chen, H. Zhang, *Chem. Rev.* **2018**, *118*, 6409; c) C. F. Markwalter, A. G. Kantor, C. P. Moore, K. A. Richardson, D. W. Wright, *Chem. Rev.* **2018**, *119*, 1456.
2. S. Roy, Z. Liu, X. Sun, M. Gharib, H. Yan, Y. Huang, S. Megahed, M. Schnabel, D. Zhu, N. Feliu, I. Chakraborty, C. Sanchez-Cano, A. M. Alkilany, W. J. Parak, *Bioconjug. Chem.* **2019**, *30*, 2751–2762.
3. M. Faraday, *Phil. Trans. R. Soc. Lond.* **1857**, *147*, 145.
4. M. Grzelczak, J. Perez-Juste, P. Mulvaney, L. M. Liz-Marzan, *Chem. Soc. Rev.* **2008**, *37*, 1783.
5. a) I. Chakraborty, T. Pradeep, *Chem. Rev.* **2017**, *117*, 8208; b) R. Jin, C. Zeng, M. Zhou, Y. Chen, *Chem. Rev.* **2016**, *116*, 10346.
6. M. Galchenko, A. Black, L. Heymann, C. Klinke, *Adv. Mater.* **2019**, *31*, 1900684.
7. V. Albano, P. Bellon, M. Manassero, M. Sansoni, *J. Chem. Soc. D: Chem. Commun.* **1970**, 1210.
8. J. Van der Velden, F. Vollenbroek, J. Bour, P. Beurskens, J. Smits, W. Bosnian, *Recueil des Travaux Chimiques des Pays-Bas* **1981**, *100*, 148.
9. G. Schmid, R. Pfeil, R. Boese, F. Bandermann, S. Meyer, G. H. M. Calis, J. W. A. van der Velden, *Chem. Ber.* **1981**, *114*, 3634.



10. G. Schmid, R. Pugin, W. Meyer-Zaika, U. Simon, *Eur. J. Inorg. Chem.* **1999**, 1999, 2051.
11. P. D. Jadzinsky, G. Calero, C. J. Ackerson, D. A. Bushnell, R. D. Kornberg, *Science* **2007**, *318*, 430.
12. a) E. Shibu, M. H. Muhammed, T. Tsukuda, T. Pradeep, *J. Phys. Chem. C* **2008**, *112*, 12168; b) L. Dhanalakshmi, T. Udayabhaskararao, T. Pradeep, *Chem. Commun.* **2012**, *48*, 859; c) I. Chakraborty, T. Udayabhaskararao, T. Pradeep, *Chem. Commun.* **2012**, *48*, 6788; d) K. Zheng, X. Yuan, K. Kuah, Z. Luo, Q. Yao, Q. Zhang, J. Xie, *Chem. Commun.* **2015**, *51*, 15165.
13. Y. Yu, Z. Luo, Y. Yu, J. Y. Lee, J. Xie, *ACS nano* **2012**, *6*, 7920.
14. T. U. B. Rao, B. Nataraju, T. Pradeep, *J. Am. Chem. Soc.* **2010**, *132*, 16304.
15. a) M. S. Bootharaju, V. M. Burlakov, T. M. Besong, C. P. Joshi, L. G. AbdulHalim, D. M. Black, R. L. Whetten, A. Goriely, O. M. Bakr, *Chem. Mater.* **2015**, *27*, 4289; b) C. Zeng, H. Qian, T. Li, G. Li, N. L. Rosi, B. Yoon, R. N. Barnett, R. L. Whetten, U. Landman, R. Jin, *Angew. Chem. Int. Ed.* **2012**, *51*, 13114.
16. T. G. Schaaff, G. Knight, M. N. Shafiqullin, R. F. Borkman, R. L. Whetten, *J. Phys. Chem. B* **1998**, *102*, 10643.
17. a) Y. Negishi, Y. Takasugi, S. Sato, H. Yao, K. Kimura, T. Tsukuda, *J. Am. Chem. Soc.* **2004**, *126*, 6518; b) Y. Negishi, K. Nobusada, T. Tsukuda, *J. Am. Chem. Soc.* **2005**, *127*, 5261.
18. a) T. Vosch, Y. Antoku, J. C. Hsiang, C. I. Richards, J. I. Gonzalez, R. M. Dickson, *Proc. Natl. Acad. Sci. U. S. A.* **2007**, *104*, 12616; b) J. T. Petty, J. Zheng, N. V. Hud, R. M. Dickson, *J. Am. Chem. Soc.* **2004**, *126*, 5207; c) J. T. Petty, C. Fan, S. P. Story, B. Sengupta, A. St. John Iyer, Z. Prudowsky, R. M. Dickson, *J. Phys. Chem. Lett.* **2010**, *1*, 2524.
19. J. Xie, Y. Zheng, J. Y. Ying, *J. Am. Chem. Soc.* **2009**, *131*, 888.
20. a) I. Chakraborty, A. Govindarajan, J. Erusappan, A. Ghosh, T. Pradeep, B. Yoon, R. L. Whetten, U. Landman, *Nano letters* **2012**, *12*, **5861**; b) I. Chakraborty, S. Bag, U. Landman, T. Pradeep, *J. Phys. Chem. Lett.* **2013**, *4*, 2769; c) I. Chakraborty, W. Kurashige, K. Kanehira, L. Gell, H. Häkkinen, Y. Negishi, T. Pradeep, *J. Phys. Chem. Lett.* **2013**, *4*, 3351; d) A. Ganguly, I. Chakraborty, T. Udayabhaskararao, T. Pradeep, *J. Nanopart. Res.* **2013**, *15*, 1522.
21. I. Chakraborty, R. G. Bhui, S. Bhat, T. Pradeep, *Nanoscale* **2014**, *6*, 8561.
22. I. Chakraborty, J. Erusappan, A. Govindarajan, K. Sugi, T. Udayabhaskararao, A. Ghosh, T. Pradeep, *Nanoscale* **2014**, *6*, 8024.
23. I. Chakraborty, S. Mahata, A. Mitra, G. De, T. Pradeep, *Dalton Trans.* **2014**, *43*, 17904.
24. S. Sarkar, I. Chakraborty, M. K. Panwar, T. Pradeep, *J. Phys. Chem. Lett.* **2014**, *5*, 3757.
25. M. Zhu, C. M. Aikens, F. J. Hollander, G. C. Schatz, R. Jin, *J. Am. Chem. Soc.* **2008**, *130*, 5883.
26. H. Qian, W. T. Eckenhoff, Y. Zhu, T. Pintauer, R. Jin, *J. Am. Chem. Soc.* **2010**, *132*, 8280.
27. A. Das, T. Li, K. Nobusada, Q. Zeng, N. L. Rosi, R. Jin, *J. Am. Chem. Soc.* **2012**, *134*, 20286.
28. C. Zeng, T. Li, A. Das, N. L. Rosi, R. Jin, *J. Am. Chem. Soc.* **2013**, *135*, 10011.
29. Y. Chen, C. Zeng, C. Liu, K. Kirschbaum, C. Gayathri, R. R. Gil, N. L. Rosi, R. Jin, *J. Am. Chem. Soc.* **2015**, *137*, 10076.
30. A. Das, C. Liu, H. Y. Byun, K. Nobusada, S. Zhao, N. Rosi, R. Jin, *Angew. Chem. Int. Ed.* **2015**, *54*, 3140.
31. C. Zeng, C. Liu, Y. Chen, N. L. Rosi, R. Jin, *J. Am. Chem. Soc.* **2016**, *138*, 8710.
32. Y. Du, H. Sheng, D. Astruc, M. Zhu, *Chem. Rev.* **2019**.
33. a) H. W. Duan, S. M. Nie, *J. Am. Chem. Soc.* **2007**, *129*, 2412; b) H. Qian, M. Zhu, E. Lanni, Y. Zhu, M. E. Bier, R. Jin, *J. Phys. Chem. C* **2009**, *113*, 17599; c) Y. Shichibu, Y. Negishi, H. Tsunoyama, M. Kanehara, T. Teranishi, T. Tsukuda, *Small* **2007**, *3*, 835.
34. T. Shimizu, T. Teranishi, S. Hasegawa, M. Miyake, *J. Phys. Chem. B* **2003**, *107*, 2719.
35. a) R. Tsunoyama, H. Tsunoyama, P. Pannopard, J. Limtrakul, T. Tsukuda, *J. Phys. Chem. C* **2010**, *114*, 16004; b) M. S. Devadas, K. Kwak, J.-W. Park, J.-H. Choi, C.-H. Jun, E. Sinn, G. Ramakrishna, D. Lee, *J. Phys. Chem. Lett.* **2010**, *1*, 1497.
36. S. Gaur, J. T. Miller, D. Stellwagen, A. Sanampudi, C. S. Kumar, J. J. Spivey, *Phys. Chem. Chem. Phys.* **2012**, *14*, 1627.
37. a) Z. Wu, J. Suhan, R. Jin, *J. Mater. Chem.* **2009**, *19*, 622; b) R. Jin, H. Qian, Z. Wu, Y. Zhu, M. Zhu, A. Mohanty, N. Garg, *J. Phys. Chem. Lett.* **2010**, *1*, 2903.
38. A. Ghosh, T. Udayabhaskararao, T. Pradeep, *J. Phys. Chem. Lett.* **2012**, *3*, 1997.
39. a) P. L. Xavier, K. Chaudhari, P. K. Verma, S. K. Pal, T. Pradeep, *Nanoscale* **2010**, *2*, 2769; b) A. Mathew, P. Sajanlal, T. Pradeep, *J. Mater. Chem.* **2011**, *21*, 11205.
40. a) G. Schmid, *Chem. Soc. Rev.* **2008**, *37*, 1909; b) G. Schmid, R. Pugin, J.-O. Malm, J.-O. Bovin, *Eur. J. Inorg. Chem.* **1998**, 1998, 813.
41. a) L. A. Pretzer, Q. X. Nguyen, M. S. Wong, *J. Phys. Chem. C* **2010**, *114*, 21226; b) B. Wu, N. Zheng, G. Fu, *Chem. Commun.* **2011**, *47*, 1039; c) J. Wu, A. Gross, H. Yang, *Nano Lett.* **2011**, *11*, 798.
42. a) J. M. Pettibone, J. W. Hudgens, *ACS nano* **2011**, *5*, 2989; b) J. M. Pettibone, J. W. Hudgens, *J. Phys. Chem. Lett.* **2010**, *1*, 2536.
43. M. Zhu, E. Lanni, N. Garg, M. E. Bier, R. Jin, *J. Am. Chem. Soc.* **2008**, *130*, 1138.
44. a) D. T. Miles, R. W. Murray, *Anal. Chem.* **2003**, *75*, 1251; b) E. S. Shibu, T. Pradeep, *Int. J. Nanosci.* **2009**, *8*, 223; c) M. S. Devadas, S. Bairu, H. Qian, E. Sinn, R. Jin, G. Ramakrishna, *J. Phys. Chem. Lett.* **2011**, *2*, 2752.
45. P. Maity, S. Xie, M. Yamauchi, T. Tsukuda, *Nanoscale* **2012**, *4*, 4027.
46. a) Y. Li, H. Cheng, T. Yao, Z. Sun, W. Yan, Y. Jiang, Y. Xie, Y. Sun, Y. Huang, S. Liu, *J. Am. Chem. Soc.* **2012**, *134*, 17997; b) S.-F. Yuan, Z.-J. Guan, W.-D. Liu, Q.-M. Wang, *Nat. Commun.* **2019**, *10*, 1.
47. M. Brust, M. Walker, D. Bethell, D. J. Schiffrin, R. Whyman, *J. Chem. Soc., Chem. Commun.* **1994**, *1*, 801.
48. a) P. J. Goulet, R. B. Lennox, *J. Am. Chem. Soc.* **2010**, *132*, 9582; b) S. R. K. Perala, S. Kumar, *Langmuir* **2013**, *29*, 9863; c) S. G. Booth, A. Uehara, S.-Y. Chang, C. La Fontaine, T. Fujii, Y. Okamoto, T. Imai, S. L. Schroeder, R. Dryfe, *Chem. Sci.* **2017**, *8*, 7954.
49. Y. Li, O. Zaluzhna, B. Xu, Y. Gao, J. M. Modest, Y. J. Tong, *J. Am. Chem. Soc.* **2011**, *133*, 2092.
50. a) M. R. Branham, A. D. Douglas, A. J. Mills, J. B. Tracy, P. S. White, R. W. Murray, *Langmuir* **2006**, *22*, 11376; b) Y. Song, A. S. Harper, R. W. Murray, *Langmuir* **2005**, *21*, 5492; c) H. Tsunoyama, Y. Negishi, T. Tsukuda, *J. Am. Chem. Soc.* **2006**, *128*, 6036.
51. A. Venzo, S. Antonello, J. A. Gascón, I. Guryanov, R. D. Leapman, N. V. Perera, A. Sousa, M. Zamuner, A. Zanella, F. Maran, *Anal. Chem.* **2011**, *83*, 6355.

52. Y. Chen, C. Zeng, D. R. Kauffman, R. Jin, *Nano Lett.* **2015**, *15*, 3603.
53. B. Bhattarai, I. Chakraborty, B. E. Conn, A. Atnagulov, T. Pradeep, T. P. Bigioni, *J. Phys. Chem. C* **2017**, *121*, 10964.
54. Z. Luo, V. Nachammai, B. Zhang, N. Yan, D. T. Leong, D.-e. Jiang, J. Xie, *J. Am. Chem. Soc.* **2014**, *136*, 10577.
55. Y. Yu, X. Chen, Q. Yao, Y. Yu, N. Yan, J. Xie, *Chem. Mater.* **2013**, *25*, 946.
56. T. Chen, J. Xie, *Chem. Rec.* **2016**, *16*, 1761.
57. P. L. Xavier, K. Chaudhari, A. Baksi, T. Pradeep, *Nano Rev.* **2012**, *3*, 14767.
58. J. S. Mohanty, A. Baksi, H. Lee, T. Pradeep, *RSC Adv.* **2015**, *5*, 48039.
59. X. Yuan, M. I. Setyawati, A. S. Tan, C. N. Ong, D. T. Leong, J. Xie, *NPG Asia Mater* **2013**, *5*, e39.
60. a) K. Pyo, V. D. Thanthirige, K. Kwak, P. Pandurangan, G. Ramakrishna, D. Lee, *J. Am. Chem. Soc.* **2015**, *137*, 8244; b) R. Tian, S. Zhang, M. Li, Y. Zhou, B. Lu, D. Yan, M. Wei, D. G. Evans, X. Duan, *Adv. Funct. Mater.* **2015**, *25*, 5006.
61. N. Goswami, F. Lin, Y. Liu, D. T. Leong, J. Xie, *Chem. Mater.* **2016**, *28*, 4009.
62. a) K. Zheng, X. Yuan, N. Goswami, Q. Zhang, J. Xie, *RSC Adv.* **2014**, *4*, 60581; b) G. Li, R. Jin, *Acc. Chem. Res.* **2013**, *46*, 1749; c) S. Yamazoe, K. Koyasu, T. Tsukuda, *Acc. Chem. Res.* **2013**, *47*, 816; d) S. Knoppe, T. Bürgi, *Acc. Chem. Res.* **2014**, *47*, 1318; e) Y. Pei, X. C. Zeng, *Nanoscale* **2012**, *4*, 4054; f) S. Malola, L. Lehtovaara, H. Häkkinen, *J. Phys. Chem. Lett.* **2014**, *5*, 1329.
63. a) T. G. Schaaff, R. L. Whetten, *J. Phys. Chem. B* **1999**, *103*, 9394; b) N. K. Chaki, Y. Negishi, H. Tsunoyama, Y. Shichibu, T. Tsukuda, *J. Am. Chem. Soc.* **2008**, *130*, 8608.
64. a) H. Qian, R. Jin, *Nano Lett.* **2009**, *9*, 4083; b) H. Qian, Y. Zhu, R. Jin, *ACS nano* **2009**, *3*, 3795; c) H. Qian, Y. Zhu, R. Jin, *Proc. Natl. Acad. Sci.* **2012**, *109*, 696.
65. C. Zeng, C. Liu, Y. Pei, R. Jin, *ACS nano* **2013**, *7*, 6138.
66. M. S. Bootharaju, C. P. Joshi, M. J. Alhilaly, O. M. Bakr, *Chem. Mater.* **2016**, *28*, 3292.
67. C. Zeng, Y. Chen, A. Das, R. Jin, *J. Phys. Chem. Lett.* **2015**, *6*, 2976.
68. B. Adhikari, A. Banerjee, *Chem. Mater.* **2010**, *22*, 4364.
69. M. A. H. Muhammed, F. Aldeek, G. Palui, L. Trapiella-Alfonso, H. Mattoussi, *ACS Nano* **2012**, *6*, 8950.
70. L. Zhu, M. Gharib, C. Becker, Y. Zeng, A. R. Ziefuß, L. Chen, A. M. Alkilany, C. Rehbock, S. Barcikowski, W. J. Parak, *J. Chem. Educ.* **2020**, *97*, 239.
71. M. van der Linden, A. J. van Bunningen, M. U. Delgado-Jaime, B. Detlefs, P. Glatzel, A. Longo, F. M. de Groot, *J. Phys. Chem. C* **2018**, *122*, 28351.
72. H. Qian, W. T. Eckenhoff, M. E. Bier, T. Pintauer, R. Jin, *Inorg. Chem.* **2011**, *50*, 10735.
73. L. C. McKenzie, T. O. Zaikova, J. E. Hutchison, *J. Am. Chem. Soc.* **2014**, *136*, 13426.
74. T. A. Dreier, C. J. Ackerson, *Angew. Chem.* **2015**, *127*, 9381.
75. M. Galchenko, R. Schuster, A. Black, M. Riedner, C. Klinke, *Nanoscale* **2019**, *11*, 1988.
76. R. L. Whetten, J. T. Khoury, M. M. Alvarez, S. Murthy, I. Vezmar, Z. L. Wang, P. W. Stephens, C. L. Cleveland, W. D. Luedtke, U. Landman, *Adv. Mater.* **1996**, *8*, 428.
77. S. Kumar, R. Jin, *Nanoscale* **2012**, *4*, 4222.
78. Y. Niihori, M. Matsuzaki, T. Pradeep, Y. Negishi, *J. Am. Chem. Soc.* **2013**, *135*, 4946.
79. Y. Niihori, C. Uchida, W. Kurashige, Y. Negishi, *Phys. Chem. Chem. Phys.* **2016**, *18*, 4251.
80. S. Tian, Y.-Z. Li, M.-B. Li, J. Yuan, J. Yang, Z. Wu, R. Jin, *Nat. Commun.* **2015**, *6*, 8667.
81. A. Ghosh, J. Hassinen, P. Pulkkinen, H. Tenhu, R. H. A. Ras, T. Pradeep, *Anal. Chem.* **2014**, *86*, 12185.
82. a) L. AbdulHalim, S. Ashraf, K. Katsiev, A. Kirmani, N. Kothalawala, D. Anjum, S. Abbas, A. Amassian, F. Stellacci, A. Dass, I. Hussain, O. Bakr, *J. Mater. Chem. A* **2013**, *1*, 10148; b) G. n. Plascencia-Villa, B. Demeler, R. L. Whetten, W. P. Griffith, M. Alvarez, D. M. Black, M. José-Yacamán, *J. Phys. Chem. C* **2016**, *120*, 8950.
83. R. Balasubramanian, R. Guo, A. J. Mills, R. W. Murray, *J. Am. Chem. Soc.* **2005**, *127*, 8126.
84. M. Zhu, H. Qian, X. Meng, S. Jin, Z. Wu, R. Jin, *Nano letters* **2011**, *11*, 3963.
85. C. Zeng, Y. Chen, G. Li, R. Jin, *Chem. Mater.* **2014**, *26*, 2635.
86. a) S. Wang, X. Meng, A. Das, T. Li, Y. Song, T. Cao, X. Zhu, M. Zhu, R. Jin, *Angew. Chem. Int. Ed.* **2014**, *53*, 2376; b) J. Lin, W. Li, C. Liu, P. Huang, M. Zhu, Q. Ge, G. Li, *Nanoscale* **2015**, *7*, 13663.
87. M. Zhu, W. T. Eckenhoff, T. Pintauer, R. Jin, *J. Phys. Chem. C* **2008**, *112*, 14221.
88. J. Fang, B. Zhang, Q. Yao, Y. Yang, J. Xie, N. Yan, *Coord. Chem. Rev.* **2016**, *322*, 1.
89. C.-A. J. Lin, T.-Y. Yang, C.-H. Lee, S. H. Huang, R. A. Sperling, M. Zanella, J. K. Li, J.-L. Shen, H.-H. Wang, H.-I. Yeh, W. J. Parak, W. H. Chang, *ACS Nano* **2009**, *3*, 395.

## AUTHOR BIOGRAPHY



**Indranath Chakraborty** earned his PhD in chemistry from the Indian Institute of Technology, Madras. He was then a postdoctoral research associate at the University of Illinois at Urbana-Champaign, IL, USA. Later, he was

an Alexander von Humboldt Postdoctoral Research Fellow at Philipps University of Marburg, Germany. Currently, he is research associate at the Center for Hybrid Nanostructure, University of Hamburg, Germany. His research area primarily focused on surface engineering of nanoparticles and atomically precise metal nanoclusters.

**How to cite this article:** Gharib M, Galchenko M, Klinke C, Parak WJ, Chakraborty I. Mechanistic insights and selected synthetic routes of atomically precise metal nanoclusters. *Nano Select.* **2021**;2:831-846.

<https://doi.org/10.1002/nano.202000210>